

# Splitting of point defect energy levels in wurtzite crystals under uniaxial stresses applied along arbitrary directions

E. McGlynn\* and M. O. Henry

*School of Physical Sciences, National Centre for Plasma Science and Technology, Dublin City University, Glasnevin, Dublin 9, Ireland*

(Received 3 August 2007; published 12 November 2007)

The splitting patterns of point defect energy levels in wurtzite crystals under uniaxial stress are derived for stress applied along an arbitrary crystal direction. The nonsymmorphic wurtzite crystal has a hexagonal point group  $C_{6v}$ , while point defects in the crystal belong to one of either the trigonal ( $C_{3v}$  and  $C_3$ ), monoclinic ( $C_{1h}$ ), or triclinic ( $C_1$ ) symmetry classes. Trigonal defects may possess both intrinsic and orientational degeneracies (apart from time-reversal degeneracy), while the monoclinic and triclinic defects possess only orientational degeneracy (again neglecting time-reversal degeneracy). The splitting patterns of the energy levels of defects belonging to these classes are derived for uniaxial stress along arbitrary directions and the contributions to the various stress-split components from the different inequivalent orientations are indicated. The results of the theoretical analyses are compared with a selection of experimental results from the literature and good agreement is found in all cases. The general equations provided here should prove to be very valuable for the interpretation of uniaxial stress data for all wurtzite crystals.

DOI: [10.1103/PhysRevB.76.184109](https://doi.org/10.1103/PhysRevB.76.184109)

PACS number(s): 78.20.Hp, 07.35.+k, 78.55.Et, 78.20.-e

## I. INTRODUCTION

Semiconductors crystallizing in the wurtzite space group such as GaN and ZnO have assumed positions of increasing technological importance in photonics and optoelectronics in the past decade.<sup>1-4</sup> This increasing technological importance has led to many studies of point and other defects in these materials for the purpose of understanding the nature of these defects and, particularly, their effects on doping.<sup>5-7</sup> Comparisons of experimental results with theoretical predictions of defect structures have been reported, including a limited number of optical studies of point defects under hydrostatic and uniaxial stress, in order to study the defect symmetry and compare the observed shift rates and symmetries with those predicted for computationally derived structures.<sup>8-10</sup> In addition, important recent (and more established) results indicate that effective routes to  $p$ -type doping in ZnO may rely primarily on defect complexes rather than isolated substitutional defects,<sup>11-13</sup> and this may explain the rather checkered history of success of  $p$ -type doping methods in ZnO. Defect complexes by their nature tend to have lower point group symmetry compared to substitutional dopants, and the experimental identification of the symmetry of these complex structures and their relationship to computationally predicted structures will be extremely important in assessing the effectiveness of proposed defect complex  $p$ -type doping methods.<sup>11-13</sup>

The uniaxial stress technique (also known as piezospectroscopy) is a powerful technique for optical spectroscopic studies of defects in crystals and can enable unambiguous identification of defect symmetries and yield values for stress shift rates (including hydrostatic shift rates) which can be compared to predictions from *ab initio* computational studies, particularly in the case of local vibrational mode spectroscopy. The technique is particularly powerful where the optical spectra of defects display narrow lines because stress-induced shifts and splittings can be clearly determined, and thus is potentially very useful for defects in, e.g., high quality single crystals of ZnO.<sup>1</sup>

In spite of the wealth of useful information which can be obtained using this technique, there are relatively few optical spectroscopic studies of wurtzite crystals under uniaxial stress compared to cubic crystals. There are a number of reports on the variation of electrical parameters with uniaxial stress<sup>14,15</sup> and of the effects of biaxial and inhomogeneous stresses on thin film properties.<sup>16,17</sup> A number of authors have reported the behavior of the ZnO near band-edge free exciton luminescence and/or reflectance under uniaxial stress applied along high symmetry directions.<sup>18,19</sup> In parallel, detailed group-theoretical analyses have appeared describing the free exciton behavior where orientational degeneracy effects are not present.<sup>20</sup> In one of these reports on ZnO, a shallow bound exciton luminescence feature has also been observed and its stress behavior reported, though not analyzed.<sup>19</sup> Apart from free exciton studies, however, there have been very few reports of uniaxial stress optical studies specifically on point defects in wurtzite crystals, where both intrinsic and orientational degeneracies may be present, and the reports which have appeared have been concentrated on the effects of uniaxial stress applied along the highest symmetry directions in the crystal only.<sup>9,10,21-23</sup> The analyses of the splitting patterns obtained have concentrated on the main features such as removal of orientational degeneracy in order to deduce the symmetry. To date, there has been no analysis of the relationships between the shift rates of the stress-split components and the number of independent parameters needed to fully describe these splittings and shift rates for defects in wurtzite crystals, using symmetry and group-theoretical methods, for stress along an arbitrary crystal direction. For defects in other hexagonal crystals, such as sapphire, a partial study of these stress pattern relationships has been reported for chromium ion pair defects but only for stresses perpendicular to the  $c$  axis along high symmetry directions in the basal plane.<sup>24,25</sup>

Bearing in mind the potential importance of defect symmetry identification to the assessment of potential  $p$ -type doping methods and the lack of a detailed, general analysis

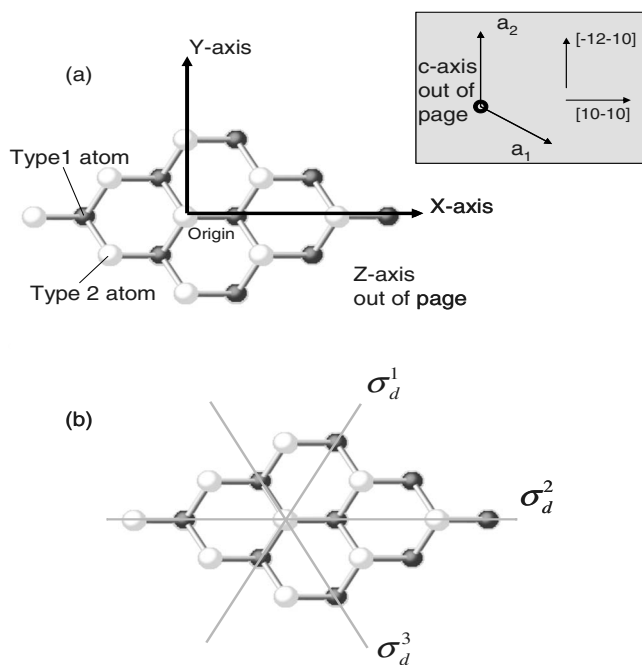


FIG. 1. (a) Top view (along the  $c$  axis direction) of the wurtzite crystal. The  $X$ ,  $Y$ , and  $Z$  axes referred to in the text are shown. The inset shows the standard hexagonal basis vectors in the basal plane and two orthogonal directions in the basal plane specified by the Miller-Bravais notation. (b) Top view (along the  $c$  axis direction) of the wurtzite crystal showing the family of  $\sigma_d^i$  reflection planes referred to in the text. The images were created using CrystalMaker, a crystal and/or molecular structure program for Mac and Windows (Ref. 48).

of the effects of stress on point defects in wurtzite crystals commented upon above, a general analysis of the expected splitting patterns of energy levels of defects in wurtzite crystals for uniaxial stresses applied along arbitrary crystal directions, similar to those undertaken for cubic crystals by our group and other workers,<sup>26–29</sup> would therefore be very useful for convenient comparison with, and interpretation of, experimental data. A general analysis of this nature would also be particularly timely as research attention shifts to the growth of wurtzite semiconductor thin films with nonpolar and mixed polarity surfaces, e.g., in order to improve device performance,<sup>30–32</sup> where the applied stress in uniaxial stress studies will most likely be along directions other than the  $c$  axis or basal plane axes, particularly in the latter case of mixed polarity surfaces.

The purpose of this paper is therefore to provide a general analysis, by the application of group-theoretical considerations, of splitting patterns of energy levels (electronic or local vibrational) of point defects in wurtzite crystals for uniaxial stresses applied along arbitrary crystal directions. The results of these analyses are compared with experimental data from sources in the literature,<sup>10</sup> and in all cases, good agreement is found between the theoretical results and a variety of experimental data.

The analyses contained in this paper may be used in the first instance to ascertain the defect symmetry, from which

more detailed models which describe the (polarized) intensity patterns of transitions and the stress-induced interactions between levels can be generated and from which more detailed information on the nature of the spectroscopic transitions and interacting states may be obtained. Accurate determination of the defect symmetry will also enable easy comparison with proposed defect structures generated by computational studies of defect formation.

## II. THEORETICAL OUTLINE

We use an orthonormal Cartesian coordinate system in the wurtzite crystal for the specification of both the applied stress direction (by giving the direction cosines or a constant multiple thereof;  $\alpha$ ,  $\beta$ , and  $\gamma$ ) and the components of the stress tensor ( $S_{ij}$ ). The Cartesian set of axes is shown in Fig. 1(a). We choose  $Z$  parallel to  $[0001]$  and  $X$  and  $Y$  parallel to  $[10-10]$  and  $[-12-10]$  (Miller-Bravais notation), respectively. The relationships between the stress direction specified with respect to the Cartesian axes (in terms of  $\alpha$ ,  $\beta$ , and  $\gamma$ ) and with respect to the conventional hexagonal basis using three indices (Miller notation; specified by  $U$ ,  $V$ , and  $W$ ) are given below in Eq. (1), where  $a$  and  $c$  are the lattice constants of the wurtzite lattice parallel and perpendicular to the basal plane, respectively. The relationship between the three index hexagonal Miller notation and the four index hexagonal Miller-Bravais notation (specified by  $u$ ,  $v$ ,  $t$ , and  $w$ ) for directions is given in standard textbooks.<sup>33</sup>

$$\begin{pmatrix} \alpha \\ \beta \\ \gamma \end{pmatrix} = \begin{pmatrix} \sqrt{3}a/2 & 0 & 0 \\ -a/2 & a & 0 \\ 0 & 0 & c \end{pmatrix} \begin{pmatrix} U \\ V \\ W \end{pmatrix}. \quad (1)$$

The effect of inequivalent defect orientations with respect to the applied stress is dealt with by assuming a single fixed defect (thus fixing the form of the stress potential in terms of the stress tensor components) and applying the operations of the full point group of the wurtzite structure ( $C_{6v}$ ) to the stress direction vector to generate 12 inequivalent uniaxial stress direction vectors. This procedure is entirely equivalent to fixing the stress direction and generating inequivalent defect orientations by applying group operators to the local defect axes. The stress tensor components corresponding to each of these stress directions are then used with the stress potential of the fixed defect to calculate the shifts and/or splitting of the energy levels. For defects with a symmetry higher than triclinic, some of these stress directions will yield identical results, i.e., orientational degeneracy.

For a stress applied along a direction with Cartesian direction cosines  $(\alpha, \beta, \gamma)$ , the full set of associated inequivalent stress directions is given in Eq. (2) below (numbered 1–12), and each is labeled with the group operation which generated this direction from the original  $(\alpha, \beta, \gamma)$  direction.

$$C_{6v} = \begin{pmatrix} \alpha, \beta, \gamma \\ -\alpha, -\beta, \gamma \\ \{-\alpha/2 - \beta\sqrt{3}/2\}, \{\alpha\sqrt{3}/2 - \beta/2\}, \gamma \\ \{-\alpha/2 + \beta\sqrt{3}/2\}, \{-\alpha\sqrt{3}/2 - \beta/2\}, \gamma \\ \{\alpha/2 + \beta\sqrt{3}/2\}, \{-\alpha\sqrt{3}/2 + \beta/2\}, \gamma \\ \{\alpha/2 - \beta\sqrt{3}/2\}, \{\alpha\sqrt{3}/2 + \beta/2\}, \gamma \\ \{-\alpha/2 + \beta\sqrt{3}/2\}, \{\alpha\sqrt{3}/2 + \beta/2\}, \gamma \\ \alpha, -\beta, \gamma \\ \{-\alpha/2 - \beta\sqrt{3}/2\}, \{-\alpha\sqrt{3}/2 + \beta/2\}, \gamma \\ \{\alpha/2 - \beta\sqrt{3}/2\}, \{-\alpha\sqrt{3}/2 - \beta/2\}, \gamma \\ \{\alpha/2 + \beta\sqrt{3}/2\}, \{\alpha\sqrt{3}/2 - \beta/2\}, \gamma \\ -\alpha, \beta, \gamma \end{pmatrix} \begin{pmatrix} 1 - E \\ 2 - C_2 \\ 3 - C_3^{-1} \\ 4 - C_3 \\ 5 - C_6 \\ 6 - C_6^{-1} \\ 7 - \sigma_d^1 \\ 8 - \sigma_d^2 \\ 9 - \sigma_d^3 \\ 10 - \sigma_v^1 \\ 11 - \sigma_v^2 \\ 12 - \sigma_v^3 \end{pmatrix}. \quad (2)$$

The rotations ( $C_2, C_3, C_3^{-1}, C_6, C_6^{-1}$ ) are about the  $Z$  axis. In the wurtzite lattice, the  $C_2, C_6,$  and  $C_6^{-1}$  operations are associated with a displacement of  $c/2$  along the  $Z$  direction;<sup>34</sup> however, this does not affect the calculation of stress directions. One of the set of reflection operations  $\sigma_d^i$  shown in Fig. 1(b), the operation labeled  $\sigma_d^2$ , corresponds to a reflection plane coincident with the  $X$ - $Z$  plane. The other members of this set are at  $120^\circ$  intervals. The set of reflections  $\sigma_v^i$  is located between the  $\sigma_d^i$  planes and is also associated with a displacement of  $c/2$  along the  $Z$  direction. Operations containing the  $c/2$  displacement cannot form part of the point group of a point defect in the crystal, as mentioned below.

The 12 rows in the matrix  $C_{6v}$  correspond to the 12 inequivalent ( $x, y, z$ )-type directions for a wurtzite crystal. The stress tensor components  $S_{ij}$  are defined by

$$S_{ij} = |S| \cos(S, i) \cos(S, j), \quad i, j \in X, Y, Z, \quad (3)$$

where  $|S|$  is the magnitude of the applied stress and  $\cos(S, i)$  is the cosine of the angle between the direction of the stress vector  $S$  and the  $i$ th crystal axis. The orthonormal crystal axes  $X, Y,$  and  $Z$  are defined in component notation as

$$X = \begin{pmatrix} 1 \\ 0 \\ 0 \end{pmatrix} \quad Y = \begin{pmatrix} 0 \\ 1 \\ 0 \end{pmatrix} \quad Z = \begin{pmatrix} 0 \\ 0 \\ 1 \end{pmatrix} \quad (4)$$

The values of the stress tensor components can be calculated using the intermediate matrices  $S_j$  as follows (where “\*” denotes ordinary matrix multiplication):

$$\begin{aligned} S_X &= C_{6v} * X, \\ S_Y &= C_{6v} * Y, \\ S_Z &= C_{6v} * Z. \end{aligned} \quad (5)$$

The  $S_{ij}$  stress tensor is calculated using the element by element array product as defined in MATLAB® (Ref. 35) (denoted by “\*\*,” below) of the  $S_i$  and  $S_j$  matrices from Eq. (5) above.

$$S_{ij} = S_i * ** S_j, \quad i, j \in X, Y, Z. \quad (6)$$

For all the point defect classes we consider (trigonal, monoclinic, and triclinic), the defect axes of one defect orientation can be aligned with the crystal axes  $X, Y,$  and  $Z,$  as indicated below, and thus the transformation properties of the stress tensor components can be identified from standard tables on group theory.<sup>36</sup> We therefore use this orientation as the fixed defect orientation for that class of defects and consider stresses along the 12 inequivalent directions [Eq. (2) above]. Using the general principles outlined by Kaplyanski<sup>26</sup> and Mohammed *et al.*,<sup>28</sup> we note that the effect of an applied stress on a defect can be written in terms of the stress potential. Different level shifts and/or splittings will in general result from the 12 inequivalent directions and these provide the full information on the splitting pattern of the ensemble of inequivalent defects under the applied stress.

### III. RESULTS

The nonsymmorphic wurtzite crystal has a hexagonal point group  $C_{6v}$ .<sup>34</sup> The  $C_2, C_6, C_6^{-1}, \sigma_v^1, \sigma_v^2,$  and  $\sigma_v^3$  operations of the  $C_{6v}$  group are all associated with a  $c/2$  displacement operation parallel to the  $c$ -axis direction of the wurtzite lattice, and thus no point in the lattice is left fixed under such operations and therefore groups containing these operations cannot be associated with point defects in the wurtzite structure (this may be contrasted with certain glide operations such as the inversion operation in the nonsymmorphic diamond lattice). Thus, point defects in the crystal belong to one of either the trigonal ( $C_{3v}$  and  $C_3$ ), monoclinic ( $C_{1h}$ ), or triclinic ( $C_1$ ) classes. Trigonal defects may possess both intrinsic (orbital, sometimes called electronic) and orientational degeneracies (apart from time-reversal degeneracy). Monoclinic and triclinic defects possess only orientational degeneracy (again neglecting time-reversal degeneracy). The origin of coordinates of the wurtzite lattice is generally chosen not at an atomic position, but for the lower symmetry groups associated with point defects, we can choose the origin of coordinates to be coincident with an atomic position, as shown in Fig. 1(a). In all cases, we use the notation and conventions for the group representations given in Ref. 36. The MATLAB® files used for the computation of the shift rates for all defect symmetry classes can be obtained by contacting the corresponding author.

#### A. Trigonal defects

There are two groups in the trigonal class ( $C_{3v}$  and  $C_3$ ). The local trigonal defect axes naturally align with the lattice axes and the data from Ref. 36 can be used directly. The symmetry elements of the defect are then  $E, C_3, C_3^{-1}, \sigma_d^1, \sigma_d^2,$  and  $\sigma_d^3$  for  $C_{3v}$  and  $E, C_3,$  and  $C_3^{-1}$  for  $C_3$ . There are two situations to be discussed for trigonal defects: (a) nondegenerate states (and Kramers' doublets) discussed in Sec. III A 1 and (b) degenerate states (not Kramers' doublets) discussed in Sec. III A 2.

### 1. Trigonal defects: Nondegenerate states (and Kramers' doublets)

For the case of nondegenerate states, only combinations of the stress tensor which transform according to the identical ( $A_1$ ) irreducible representation of the point group lead to energy shifts and the stress potential is given by Eq. (7).<sup>26,37</sup> The same considerations apply for both groups  $C_{3v}$  (representations  $A_1$  and  $A_2$ ) and  $C_3$  (representation  $A$ ) in this case, unlike the case for trigonal  $E$  states in Sec. III A 2.

$$V_{trig}^{nd} = At1 * (S_{xx} + S_{yy} + S_{zz}) + At2 * (2S_{zz} - S_{xx} - S_{yy}), \quad (7)$$

where  $At1$  and  $At2$  are operators transforming as the identical representations of the point group. When the shift rates for the defect are calculated for the 12 inequivalent stress directions for an original stress with direction cosines  $(\alpha, \beta, \gamma)$ , it is found that no splitting is seen for any stress direction. The shift rate (energy/wave number shift per unit applied stress),  $R_{trig}$ , for the level in all cases is given by

$$R_{trig}^{nd} = \frac{At1 * (\alpha^2 + \beta^2 + \gamma^2) + At2 * (2\gamma^2 - \alpha^2 - \beta^2)}{(\alpha^2 + \beta^2 + \gamma^2)}. \quad (8)$$

The hydrostatic shift rate is simply given by  $3 * At1$  (i.e., the stress potential when  $S_{xx}=S_{yy}=S_{zz}=1$ ; all other stress tensor components are zero). The nondegenerate states are not split by the application of stress, and the orientational degeneracy is not lifted for any applied stress direction. This is because

the linear combinations of stress tensor components which transform according to the  $A_1$  identical representation of the  $C_{3v}$  group [and thus contribute to the stress potential in Eq. (7)] also transform according to the  $A_1$  identical representation of the  $C_{6v}$  group. Consequently, they are invariant under all operations of the wurtzite point group (and indeed are also invariant under all operations of the larger  $C_{\infty v}$  group).<sup>36</sup> This is not the case for degenerate,  $E$ , states as shown in Sec. III A 2 below, where the effects of orientational degeneracy are seen.

For degenerate states related by time-reversal symmetry (Kramers' doublets<sup>37</sup>), the shift rate of the doublet is also given by Eq. (8). This applies to representations  $E_{1/2}$  and  $\{^1E_{3/2} \oplus ^2E_{3/2}\}$  of group  $C_{3v}$  and to representations  $\{^1E_{3/2} \oplus ^2E_{3/2}\}$  and  $\{A_{3/2} \oplus A_{3/2}\}$  of group  $C_3$ . In all cases, the dual considerations of time-reversal symmetry and the Hermiticity of the potential operator yield constraints on the matrix elements. We bear in mind that the standard theorem for a matrix element  $\langle \psi_{k'}^j, V \phi_k^j \rangle$  between functions  $\psi_{k'}^j$  and  $\phi_k^j$ , transforming according to the  $k'$  row of the  $\Gamma_{j'}$  irreducible representation and the  $k$  row of the  $\Gamma_j$  irreducible representation, respectively, under the action of a potential  $V$  (transforming according to an irreducible representation  $\Gamma_V$ ) indicates that the element is zero unless  $\Gamma_{j'}^* \times \Gamma_V \times \Gamma_j$  includes the identical representation. The interaction matrix in the space spanned by  $\{^1E_{3/2} \oplus ^2E_{3/2}\}$  in both  $C_{3v}$  and  $C_3$ , in the space spanned by  $\{A_{3/2} \oplus A_{3/2}\}$  in  $C_3$ , and in the space spanned by the irreducible representation  $E_{1/2}$  of  $C_{3v}$  is then

$$\begin{pmatrix} \begin{pmatrix} At1 * (S_{xx} + S_{yy} + S_{zz}) \\ + At2 * (2S_{zz} - S_{xx} - S_{yy}) \end{pmatrix} & 0 \\ 0 & \begin{pmatrix} At1 * (S_{xx} + S_{yy} + S_{zz}) \\ + At2 * (2S_{zz} - S_{xx} - S_{yy}) \end{pmatrix} \end{pmatrix}, \quad (9)$$

and thus the time-reversal degenerate levels shift as a pair with the same shift rate as in Eq. (8).

### 2. Trigonal defects: Degenerate states

For the case of the twofold degenerate state ( $^1E \oplus ^2E$ ) of a defect with  $C_3$  symmetry, it is not possible to analyze the splitting in a general fashion using group theory as Clebsch-Gordan coefficients are not uniquely defined in the absence of reflection planes, and the interaction matrix due to the applied potential will thus also not be uniquely defined. Hughes and Runciman have also noted this point in their discussion of trigonal defects under uniaxial stress in cubic crystals.<sup>38</sup> In the case of a twofold degenerate  $E$  state of a defect with  $C_{3v}$  symmetry, however, we can use the previously calculated stress interaction matrix<sup>39</sup> for such a system, shown in Eq. (10):

$$VW_{trig}^d = \begin{pmatrix} \begin{pmatrix} A1 * (S_{xx} + S_{yy} + S_{zz}) \\ + A2 * (2S_{zz} - S_{xx} - S_{yy}) \\ - B_1(S_{yy} - S_{xx}) - 2B_2(S_{xz}) \end{pmatrix} & \{2B_1S_{xy} + 2B_2S_{yz}\} \\ \{2B_1S_{xy} + 2B_2S_{yz}\} & \begin{pmatrix} A1 * (S_{xx} + S_{yy} + S_{zz}) \\ + A2 * (2S_{zz} - S_{xx} - S_{yy}) \\ + B_1(S_{yy} - S_{xx}) + 2B_2(S_{xz}) \end{pmatrix} \end{pmatrix}. \quad (10)$$

The original level splits into four under the action of stress along an arbitrary direction, with both orientational and electronic degeneracies lifted. There are two inequivalent orientations of the defect: (a) defect 1, associated with all operations of the  $C_{3v}$  defect point group [operations 1, 3, 4, 7, 8, and 9 in Eq. (2)], and (b) defect 2, associated with all operations of the  $C_{6v}$  lattice

point group not in the defect point group [operations 2, 5, 6, 10, 11, and 12 in Eq. (2)]. The originally twofold degenerate energy level at each defect splits and the splitting is different at defects 1 and 2. The shift rates for an applied stress with direction cosines  $(\alpha, \beta, \gamma)$  are shown in Eq. (11) below.

$$R_{defect\ 1}^{d-trig} = \frac{A1 * (\alpha^2 + \beta^2 + \gamma^2) + A2 * (2\gamma^2 - \alpha^2 - \beta^2) \pm \sqrt{[B_1^2(\alpha^4 + \beta^4 + 2\alpha^2\beta^2) + B_2^2(4\alpha^2\gamma^2 + 4\beta^2\gamma^2) + B_1B_2(12\beta^2\alpha\gamma - 4\alpha^3\gamma)]}}{(\alpha^2 + \beta^2 + \gamma^2)},$$

$$R_{defect\ 2}^{d-trig} = \frac{A1 * (\alpha^2 + \beta^2 + \gamma^2) + A2 * (2\gamma^2 - \alpha^2 - \beta^2) \pm \sqrt{[B_1^2(\alpha^4 + \beta^4 + 2\alpha^2\beta^2) + B_2^2(4\alpha^2\gamma^2 + 4\beta^2\gamma^2) - B_1B_2(12\beta^2\alpha\gamma - 4\alpha^3\gamma)]}}{(\alpha^2 + \beta^2 + \gamma^2)}.$$
(11)

The hydrostatic shift rate for such defects is given by  $3 * A1$ .

### B. Monoclinic defects

There is a single group in the monoclinic class ( $C_{1h}$ ). The local monoclinic defect axes align with the lattice axes and the data from Ref. 36 can be used, simply by noting that our  $x$  axis corresponds to the  $y$  axis in Ref. 36 and our  $z$  axis to the  $x$  axis in Ref. 36 for consistency with our choice of crystal axis labels. The symmetry elements of the defect are then  $E$  and  $\sigma_d^2$ . Defects with monoclinic symmetry display no orbital degeneracy (beyond time-reversal degeneracy) and thus the splitting of energy levels is entirely due to orientational degeneracy. Once again, only combinations of the stress tensor which transform according to the identical ( $A_1$ ) irreducible representation of the  $C_{1h}$  point group lead to energy shifts and the stress potential is given by Eq. (12).

$$V_{mono} = (Am1 * S_{xx}) + (Am2 * S_{yy}) + (Am3 * S_{zz}) + (Am4 * S_{xz}).$$
(12)

There are six inequivalent defect orientations (corresponding to the index of the  $C_{1h}$  subgroup in the  $C_{6v}$  group) and thus the line splits into six components [for an applied stress with direction cosines  $(\alpha, \beta, \gamma)$ ] with the shift rates shown below in Eq. (13). The inequivalent stress directions from Eq. (2), which contribute to each component, are shown as superscripts in parentheses on the left hand side of each equation. The case of Kramers' doublets under time-reversal symmetry is identical to that considered in Sec. III A 2 above and the doublets shift together with shift rates given in Eq. (13) below.

$$R_{mono}^{(1,8)} = \frac{(Am1 * \alpha^2) + (Am2 * \beta^2) + (Am3 * \gamma^2) + (Am4 * \alpha\gamma)}{(\alpha^2 + \beta^2 + \gamma^2)},$$

$$R_{mono}^{(2,12)} = \frac{(Am1 * \alpha^2) + (Am2 * \beta^2) + (Am3 * \gamma^2) - (Am4 * \alpha\gamma)}{(\alpha^2 + \beta^2 + \gamma^2)},$$

$$R_{mono}^{(3,9)} = \left[ \alpha^2 \left( \frac{Am1}{4} + \frac{3 * Am2}{4} \right) + \beta^2 \left( \frac{3 * Am1}{4} + \frac{Am2}{4} \right) + \gamma^2 (Am3) + \alpha\beta \left( \frac{\sqrt{3} * Am1}{2} - \frac{\sqrt{3} * Am2}{2} \right) \right. \\ \left. + \alpha\gamma \left( -\frac{Am4}{2} \right) + \beta\gamma \left( -\frac{\sqrt{3} * Am4}{2} \right) \right] / (\alpha^2 + \beta^2 + \gamma^2),$$

$$R_{mono}^{(4,7)} = \left[ \alpha^2 \left( \frac{Am1}{4} + \frac{3 * Am2}{4} \right) + \beta^2 \left( \frac{3 * Am1}{4} + \frac{Am2}{4} \right) + \gamma^2 (Am3) + \alpha\beta \left( -\frac{\sqrt{3} * Am1}{2} + \frac{\sqrt{3} * Am2}{2} \right) \right. \\ \left. + \alpha\gamma \left( -\frac{Am4}{2} \right) + \beta\gamma \left( \frac{\sqrt{3} * Am4}{2} \right) \right] / (\alpha^2 + \beta^2 + \gamma^2),$$

$$R_{mono}^{(5,11)} = \left[ \alpha^2 \left( \frac{Am1}{4} + \frac{3 * Am2}{4} \right) + \beta^2 \left( \frac{3 * Am1}{4} + \frac{Am2}{4} \right) + \gamma^2 (Am3) + \alpha\beta \left( \frac{\sqrt{3} * Am1}{2} - \frac{\sqrt{3} * Am2}{2} \right) \right. \\ \left. + \alpha\gamma \left( \frac{Am4}{2} \right) + \beta\gamma \left( \frac{\sqrt{3} * Am4}{2} \right) \right] / (\alpha^2 + \beta^2 + \gamma^2),$$

$$R_{mono}^{(6,10)} = \left[ \alpha^2 \left( \frac{Am1}{4} + \frac{3 * Am2}{4} \right) + \beta^2 \left( \frac{3 * Am1}{4} + \frac{Am2}{4} \right) + \gamma^2 (Am3) + \alpha\beta \left( -\frac{\sqrt{3} * Am1}{2} + \frac{\sqrt{3} * Am2}{2} \right) + \alpha\gamma \left( \frac{Am4}{2} \right) + \beta\gamma \left( -\frac{\sqrt{3} * Am4}{2} \right) \right] / (\alpha^2 + \beta^2 + \gamma^2). \quad (13)$$

The hydrostatic shift rate for such defects is given by  $Am1+Am2+Am3$ .

### C. Triclinic defects

Triclinic defects are defects showing no symmetry, i.e., only the identity operation leaves them unchanged. For this reason, they show no natural axis directions and one may of course choose the axis direction of the defect to coincide with the lattice axes. Defects with triclinic symmetry display no orbital degeneracy (beyond time-reversal degeneracy). The splitting of energy levels is entirely due to orientational degeneracy, and using the same approach detailed in previous sections, the stress potential is given by Eq. (14).

$$V_{triclinic} = (Atr1 * S_{xx}) + (Atr2 * S_{yy}) + (Atr3 * S_{zz}) + (Atr4 * S_{xy}) + (Atr5 * S_{xz}) + (Atr6 * S_{yz}). \quad (14)$$

There are 12 inequivalent defect orientations (corresponding to the order of the  $C_{6v}$  group) and thus the line splits into 12 components [for an original stress with direction cosines  $(\alpha, \beta, \gamma)$ ] with the shift rates shown below in Eqs. (15a) and (15b). The inequivalent stress directions from Eq. (2), which contribute to each component, are shown as superscripts in parentheses on the left hand side of each equation. The case of Kramers' doublets under time-reversal symmetry is identical to that considered previously and the splitting pattern once again is not altered.

$$R_{triclinic}^{(1)} = \frac{(Atr1 * \alpha^2) + (Atr2 * \beta^2) + (Atr3 * \gamma^2) + (Atr4 * \alpha\beta) + (Atr5 * \alpha\gamma) + (Atr6 * \beta\gamma)}{(\alpha^2 + \beta^2 + \gamma^2)},$$

$$R_{triclinic}^{(2)} = \frac{(Atr1 * \alpha^2) + (Atr2 * \beta^2) + (Atr3 * \gamma^2) + (Atr4 * \alpha\beta) - (Atr5 * \alpha\gamma) - (Atr6 * \beta\gamma)}{(\alpha^2 + \beta^2 + \gamma^2)},$$

$$R_{triclinic}^{(3)} = \left[ \alpha^2 \left( \frac{Atr1}{4} + \frac{3 * Atr2}{4} - \frac{\sqrt{3}Atr4}{4} \right) + \beta^2 \left( \frac{3 * Atr1}{4} + \frac{Atr2}{4} + \frac{\sqrt{3}Atr4}{4} \right) + \gamma^2 (Atr3) + \alpha\beta \left( \frac{\sqrt{3} * Atr1}{2} - \frac{\sqrt{3} * Atr2}{2} - \frac{Atr4}{2} \right) + \alpha\gamma \left( \frac{\sqrt{3}Atr6}{2} - \frac{Atr5}{2} \right) + \beta\gamma \left( -\frac{Atr6}{2} - \frac{\sqrt{3} * Atr5}{2} \right) \right] / (\alpha^2 + \beta^2 + \gamma^2),$$

$$R_{triclinic}^{(4)} = \left[ \alpha^2 \left( \frac{Atr1}{4} + \frac{3 * Atr2}{4} + \frac{\sqrt{3}Atr4}{4} \right) + \beta^2 \left( \frac{3 * Atr1}{4} + \frac{Atr2}{4} - \frac{\sqrt{3}Atr4}{4} \right) + \gamma^2 (Atr3) + \alpha\beta \left( -\frac{\sqrt{3} * Atr1}{2} + \frac{\sqrt{3} * Atr2}{2} - \frac{Atr4}{2} \right) + \alpha\gamma \left( -\frac{\sqrt{3}Atr6}{2} - \frac{Atr5}{2} \right) + \beta\gamma \left( -\frac{Atr6}{2} + \frac{\sqrt{3} * Atr5}{2} \right) \right] / (\alpha^2 + \beta^2 + \gamma^2),$$

$$R_{triclinic}^{(5)} = \left[ \alpha^2 \left( \frac{Atr1}{4} + \frac{3 * Atr2}{4} - \frac{\sqrt{3}Atr4}{4} \right) + \beta^2 \left( \frac{3 * Atr1}{4} + \frac{Atr2}{4} + \frac{\sqrt{3}Atr4}{4} \right) + \gamma^2 (Atr3) + \alpha\beta \left( \frac{\sqrt{3} * Atr1}{2} - \frac{\sqrt{3} * Atr2}{2} - \frac{Atr4}{2} \right) + \alpha\gamma \left( -\frac{\sqrt{3}Atr6}{2} + \frac{Atr5}{2} \right) + \beta\gamma \left( \frac{Atr6}{2} + \frac{\sqrt{3} * Atr5}{2} \right) \right] / (\alpha^2 + \beta^2 + \gamma^2),$$

$$R_{triclinic}^{(6)} = \left[ \alpha^2 \left( \frac{Atr1}{4} + \frac{3 * Atr2}{4} + \frac{\sqrt{3}Atr4}{4} \right) + \beta^2 \left( \frac{3 * Atr1}{4} + \frac{Atr2}{4} - \frac{\sqrt{3}Atr4}{4} \right) + \gamma^2 (Atr3) + \alpha\beta \left( -\frac{\sqrt{3} * Atr1}{2} + \frac{\sqrt{3} * Atr2}{2} - \frac{Atr4}{2} \right) + \alpha\gamma \left( \frac{\sqrt{3}Atr6}{2} + \frac{Atr5}{2} \right) + \beta\gamma \left( \frac{Atr6}{2} - \frac{\sqrt{3} * Atr5}{2} \right) \right] / (\alpha^2 + \beta^2 + \gamma^2), \quad (15a)$$

$$\begin{aligned}
R_{\text{triclinic}}^{(7)} &= \left[ \alpha^2 \left( \frac{\text{Atr1}}{4} + \frac{3 * \text{Atr2}}{4} - \frac{\sqrt{3}\text{Atr4}}{4} \right) + \beta^2 \left( \frac{3 * \text{Atr1}}{4} + \frac{\text{Atr2}}{4} + \frac{\sqrt{3}\text{Atr4}}{4} \right) + \gamma^2(\text{Atr3}) \right. \\
&\quad \left. + \alpha\beta \left( -\frac{\sqrt{3} * \text{Atr1}}{2} + \frac{\sqrt{3} * \text{Atr2}}{2} + \frac{\text{Atr4}}{2} \right) + \alpha\gamma \left( \frac{\sqrt{3}\text{Atr6}}{2} - \frac{\text{Atr5}}{2} \right) + \beta\gamma \left( \frac{\text{Atr6}}{2} + \frac{\sqrt{3} * \text{Atr5}}{2} \right) \right] / (\alpha^2 + \beta^2 + \gamma^2), \\
R_{\text{triclinic}}^{(8)} &= \frac{(\text{Atr1} * \alpha^2) + (\text{Atr2} * \beta^2) + (\text{Atr3} * \gamma^2) - (\text{Atr4} * \alpha\beta) + (\text{Atr5} * \alpha\gamma) - (\text{Atr6} * \beta\gamma)}{(\alpha^2 + \beta^2 + \gamma^2)}, \\
R_{\text{triclinic}}^{(9)} &= \left[ \alpha^2 \left( \frac{\text{Atr1}}{4} + \frac{3 * \text{Atr2}}{4} + \frac{\sqrt{3}\text{Atr4}}{4} \right) + \beta^2 \left( \frac{3 * \text{Atr1}}{4} + \frac{\text{Atr2}}{4} - \frac{\sqrt{3}\text{Atr4}}{4} \right) + \gamma^2(\text{Atr3}) \right. \\
&\quad \left. + \alpha\beta \left( \frac{\sqrt{3} * \text{Atr1}}{2} - \frac{\sqrt{3} * \text{Atr2}}{2} + \frac{\text{Atr4}}{2} \right) + \alpha\gamma \left( -\frac{\sqrt{3}\text{Atr6}}{2} - \frac{\text{Atr5}}{2} \right) + \beta\gamma \left( \frac{\text{Atr6}}{2} - \frac{\sqrt{3} * \text{Atr5}}{2} \right) \right] / (\alpha^2 + \beta^2 + \gamma^2), \\
R_{\text{triclinic}}^{(10)} &= \left[ \alpha^2 \left( \frac{\text{Atr1}}{4} + \frac{3 * \text{Atr2}}{4} - \frac{\sqrt{3}\text{Atr4}}{4} \right) + \beta^2 \left( \frac{3 * \text{Atr1}}{4} + \frac{\text{Atr2}}{4} + \frac{\sqrt{3}\text{Atr4}}{4} \right) + \gamma^2(\text{Atr3}) \right. \\
&\quad \left. + \alpha\beta \left( -\frac{\sqrt{3} * \text{Atr1}}{2} + \frac{\sqrt{3} * \text{Atr2}}{2} + \frac{\text{Atr4}}{2} \right) + \alpha\gamma \left( -\frac{\sqrt{3}\text{Atr6}}{2} + \frac{\text{Atr5}}{2} \right) + \beta\gamma \left( -\frac{\text{Atr6}}{2} - \frac{\sqrt{3} * \text{Atr5}}{2} \right) \right] / (\alpha^2 + \beta^2 + \gamma^2), \\
R_{\text{triclinic}}^{(11)} &= \left[ \alpha^2 \left( \frac{\text{Atr1}}{4} + \frac{3 * \text{Atr2}}{4} + \frac{\sqrt{3}\text{Atr4}}{4} \right) + \beta^2 \left( \frac{3 * \text{Atr1}}{4} + \frac{\text{Atr2}}{4} - \frac{\sqrt{3}\text{Atr4}}{4} \right) + \gamma^2(\text{Atr3}) \right. \\
&\quad \left. + \alpha\beta \left( \frac{\sqrt{3} * \text{Atr1}}{2} - \frac{\sqrt{3} * \text{Atr2}}{2} + \frac{\text{Atr4}}{2} \right) + \alpha\gamma \left( \frac{\sqrt{3}\text{Atr6}}{2} + \frac{\text{Atr5}}{2} \right) + \beta\gamma \left( -\frac{\text{Atr6}}{2} + \frac{\sqrt{3} * \text{Atr5}}{2} \right) \right] / (\alpha^2 + \beta^2 + \gamma^2), \\
R_{\text{triclinic}}^{(12)} &= \frac{(\text{Atr1} * \alpha^2) + (\text{Atr2} * \beta^2) + (\text{Atr3} * \gamma^2) - (\text{Atr4} * \alpha\beta) - (\text{Atr5} * \alpha\gamma) + (\text{Atr6} * \beta\gamma)}{(\alpha^2 + \beta^2 + \gamma^2)}. \tag{15b}
\end{aligned}$$

The hydrostatic shift rate for such defects is given by  $\text{Atr1} + \text{Atr2} + \text{Atr3}$ .

#### IV. COMPARISON WITH EXPERIMENTAL DATA IN LITERATURE

While a number of studies have appeared concerning the effects of uniaxial stress on the band-edge reflectivity (free exciton) spectra for wurtzite crystals, e.g., ZnO, as we have outlined in Sec. I above, uniaxial stress studies of point defects in wurtzite crystals are much rarer. We have referred to a number of these in Sec. I. From this group, we select a publication which reports uniaxial stress studies on the energy levels of local vibrational modes of three H-related defects in ZnO.<sup>10</sup> The spectroscopic absorption lines reported in these papers correspond to the absorption of a photon by a local defect vibrational mode causing a transition from the defect ground state (transforming as the identical  $A_1$  representation) to the excited state. The shift rate of the transition will then be the difference between the shift rates of the ground and excited states, and the analysis of Sec. III can be used in all cases with the effect of the ground state shifts simply leading to a different value of the effective stress

operators. We apply our analyses to the reported data and show that in all cases, our equations can consistently fit the data shift rates within or close to the reported accuracy ( $0.5 \text{ cm}^{-1}/\text{GPa}$ ), and are consistent with other independent measurements where available. In one instance, we are able to predict the shift rate of a weak, unobserved, component. In addition, the conclusions drawn concerning the defect symmetry from our analysis consistently match those in the original paper.

##### A. $3326 \text{ cm}^{-1}$ O-H defect<sup>10</sup>

In the case of the O-H defect reported in Ref. 10, uniaxial stress was applied along the  $[0001]$ ,  $[1-210]$ , and  $[10-10]$  directions, i.e., our  $Z$ ,  $Y$ , and  $X$  axes. The  $(\alpha, \beta, \gamma)$  components for these directions are as follows:

$$[0001] \rightarrow \alpha = \beta = 0, \quad \gamma = 1,$$

$$[1-210] \rightarrow \alpha = 0, \quad \beta = 1, \quad \gamma = 0,$$

$$[10-10] \rightarrow \alpha = 1, \quad \beta = 0, \quad \gamma = 0.$$

The authors observe no splitting under stress along  $[0001]$  and splitting into two components for stress along either

TABLE I. Summary of experimentally observed data (from Ref. 10) and fitted stress parameters [using Eqs. (8) and (13)]. The observed and predicted shift rates of the stress-split components are also tabulated.

Defect transition (cm <sup>-1</sup> ) <sup>a</sup>	Fitted stress parameters <sup>b</sup> (cm <sup>-1</sup> /GPa)	Shift rates in (cm <sup>-1</sup> /GPa) (experimental error $\sim \pm 0.5$ cm <sup>-1</sup> /GPa)					
		[0001] stress (Expt.) <sup>a</sup>	[0001] stress (Fit)	[1-210] stress (Expt.) <sup>a</sup>	[1-210] stress (Fit)	[10-10] stress (Expt.) <sup>a</sup>	[10-10] stress (Fit)
3326	$Am1 = +0.73$	0	0	-2.1	-2.2	-1.3	-1.47
Monoclinic	$Am2 = -2.2$ $Am3 = 0$			0	0	0.8	0.73
3577.3	$Ar1 = -0.1$	-2.5	-2.5	1.1	1.1	1.1	1.1
Trigonal	$Ar2 = -1.2$						
3312.2	$Am1 = +5$	-5.5	-5.5	-1.8	-1.8	-0.6	-0.1
Monoclinic	$Am1 = -1.8$ $Am3 = -5.5$			3.3	3.3	5.8	5
3349.6	$Am1 = +2.5$	2.5	2.5	-7.5	-7.5	-5.8	-5
Monoclinic	$Am2 = -7.5$ $Am3 = +2.5$			0.8	0	Unseen	2.5

<sup>a</sup>Reference 10.

<sup>b</sup>Equations (8) and (13).

[1-210] or [10-10]. We consider the various options from Sec. III above.

(1) Trigonal nondegenerate states do not split for stress along any direction; thus, the defect excited state cannot be a nondegenerate trigonal state.

(2) Trigonal  $E$  states do not split for stress parallel to [0001] and split into two components for stress along either [1-210] or [10-10]. The shift rates from Eq. (11) above are

$$[0001] \text{ stress } A1 + 2A2,$$

$$[1-210] \text{ or } [10-10] \text{ stress } A1 - A2 \pm B1.$$

(3) Monoclinic nondegenerate states do not split for stress parallel to [0001] and split into two components for stress along either [1-210] or [10-10]. The shift rates from Eq. (13) above are

$$[0001] \text{ stress } Am3,$$

$$[1-210] \text{ stress } \begin{cases} Am2 \\ (3Am1 + Am2)/4, \end{cases}$$

$$[10-10] \text{ stress } \begin{cases} Am1 \\ (3Am2 + Am1)/4. \end{cases}$$

(4) Triclinic nondegenerate states do not split for stress parallel to [0001] and split into three components for stress along either [1-210] or [10-10]; thus, the defect excited state cannot be a nondegenerate triclinic state.

Clearly, the only two options for the symmetry of this defect are (2) and (3) above. Considering the data in Ref. 10 more closely, the shift rates for the stress-split components are 0 cm<sup>-1</sup>/GPa ([0001] stress direction), 0 and

-2.1 cm<sup>-1</sup>/GPa ([1-210] stress direction), and 0.8 and -1.3 cm<sup>-1</sup>/GPa ([10-10] stress direction). The shift rates of trigonal  $E$  states from Eq. (11) above are  $A1 + 2A2$  ([0001] stress) and  $A1 - A2 \pm B1$  ([1-210] or [10-10] stress). Thus, equal shift rates are predicted for both [1-210] and [10-10] stress directions, contrary to the observed data. The only suitable option is therefore (3), i.e., that the defect is monoclinic. This is in agreement with the assignments in the literature, where the O-H defect is assigned to a single bond located close to the basal plane of the ZnO crystal, and supports the assignment that the O-H defect lies in the vertical reflection plane.<sup>10</sup> The experimental data may be consistently fitted within the stated accuracy in the paper by using Eq. (13) and choosing  $Am2 = -2.2$  cm<sup>-1</sup>/GPa,  $Am1 = +0.73$  cm<sup>-1</sup>/GPa, and  $Am3 = 0$  cm<sup>-1</sup>/GPa. Because there are four stress-split components for stress directions perpendicular to the  $z$  axis and two stress parameters, the internal consistency of the fit provides strong support for the symmetry assignment. The hydrostatic shift rate based on these parameters,  $(Am1 + Am2 + Am3) = -1.47$  cm<sup>-1</sup>/GPa, is in good agreement with the independent experimental result of Jokela and McCluskey.<sup>8</sup> The observed and predicted shift rates are summarized in Table I.

### B. 3577.3 cm<sup>-1</sup> O-H defect<sup>10</sup>

Uniaxial stress was applied along the same directions as described above in Sec. IV A. The authors observe no splitting for stress along any direction and the shift rates are -2.5 cm<sup>-1</sup>/GPa ([0001] stress direction) and +1.1 cm<sup>-1</sup>/GPa (stress direction perpendicular to [0001]). These data are consistent only with the defect having trigonal symmetry and no orbital degeneracy, i.e., option (1) in Sec. IV A above.

This is again consistent with the assignment of Lavrov and Weber.<sup>10</sup> The data can be consistently (though trivially) fitted within the experimental accuracy quoted using Eq. (8) with  $A_{t1} = -0.1 \text{ cm}^{-1}/\text{GPa}$  and  $A_{t2} = -1.2 \text{ cm}^{-1}/\text{GPa}$ . The hydrostatic shift rate is given by  $3^*A_{t1} = -0.3 \text{ cm}^{-1}/\text{GPa}$ , again in agreement with the literature. The observed and predicted shift rates are summarized in Table I.

### C. 3312.2 $\text{cm}^{-1}$ $V_{\text{Zn}}\text{-H}_2$ defect<sup>10</sup>

Uniaxial stress was again applied along the same directions as described above in Sec. IV A. The authors observe no splitting under stress along [0001] and splitting into two components for stress along either [1-210] or [10-10]. The shift rates for the stress-split components are  $-5.5 \text{ cm}^{-1}/\text{GPa}$  ([0001] stress direction),  $-1.8$  and  $3.3 \text{ cm}^{-1}/\text{GPa}$  ([1-210] stress direction), and  $-0.6$  and  $5.8 \text{ cm}^{-1}/\text{GPa}$  ([10-10] stress direction). For the same reasons as in Sec. IV A, we discount the possibility of a trigonal  $E$  state. The only suitable option therefore is that the defect is again monoclinic, in agreement with the assignments in the literature. The data can again be consistently fitted by using Eq. (13) and choosing  $Am_2 = -1.8 \text{ cm}^{-1}/\text{GPa}$ ,  $Am_1 = +5 \text{ cm}^{-1}/\text{GPa}$ , and  $Am_3 = -5.5 \text{ cm}^{-1}/\text{GPa}$ . Once again, the internal consistency of the fit provides strong support for the symmetry assignment. The hydrostatic shift rate based on these parameters is  $(Am_1 + Am_2 + Am_3) = -2.2 \text{ cm}^{-1}/\text{GPa}$ , in agreement with the estimate by Lavrov and Weber.<sup>10</sup> The observed and predicted shift rates are summarized in Table I.

### D. 3349.6 $\text{cm}^{-1}$ $V_{\text{Zn}}\text{-H}_2$ defect<sup>10</sup>

Using the same experimental conditions as for the other sections, the authors observe no splitting under stress along [0001] and either splitting into two components for stress along [1-210] or only a single component for stress along [10-10] (though this is attributed to the expected weakness of the component, below the experimental detection limit). The shift rates for the stress-split components are  $2.5 \text{ cm}^{-1}/\text{GPa}$  ([0001] stress direction),  $-7.5$  and  $0.8 \text{ cm}^{-1}/\text{GPa}$  ([1-210] stress direction), and  $-5.8 \text{ cm}^{-1}/\text{GPa}$  ([10-10] stress direction). Because the  $3349.6 \text{ cm}^{-1}$  transition is associated with the same defect complex as the  $3312.2 \text{ cm}^{-1}$  transition, clearly, the transition is at a monoclinic defect. The data can be consistently fitted within the experimental error by using Eq. (13) and choosing  $Am_2 = -7.5 \text{ cm}^{-1}/\text{GPa}$ ,  $Am_1 = +2.5 \text{ cm}^{-1}/\text{GPa}$ , and  $Am_3 = 2.5 \text{ cm}^{-1}/\text{GPa}$ .

The fit is internally consistent because the parameters  $Am_2$  and  $Am_1$  can be found from the data for [1-210] stress and they correctly predict the shift rate of the only observed feature for [10-10] stress. However, our equations also yield the shift rate of the unseen component for [10-10] stress, shown in Table I. The hydrostatic shift rate based on these parameters is  $(Am_1 + Am_2 + Am_3) = -2.5 \text{ cm}^{-1}/\text{GPa}$ , in agreement with the estimate by Lavrov and Weber.<sup>10</sup>

In all cases above, it is seen that the analysis in Sec. III can be used to immediately determine the appropriate symmetry class of the defect under study, using the number of

stress-split components and general features of the shift rate equations as a guide, and our conclusions are in full agreement with the original report. Fits of the experimental shift rates to the computed shift rates for the appropriate symmetry class yield values for the stress operators which can be used to compute the hydrostatic shift rates for the defect. Our fitted values for the stress operators yield values for the hydrostatic shift rate in agreement with both the original report by Lavrov and Weber<sup>10</sup> and also with an independent measurement of this quantity in the case of one defect discussed above. In one case, our equations have enabled us to predict the shift rate of an experimentally unseen component.

## V. DISCUSSION

The analysis of Sec. III above yields the splitting patterns and stress shift rates of the energy levels of all possible symmetry classes of point defects in the wurtzite lattice, for stress applied along an arbitrary direction. A number of further points merit a fuller discussion.

The effects of piezoelectrically induced fields (which may occur in conjunction with stresses in the technologically important wurtzite crystals) on the defect energy levels are not considered in our analyses. Comparisons with results in the literature for local defect vibrational modes in ZnO show that our analysis fits the observed data well and piezoelectrically induced fields do not appear to be of importance for such levels. In the case of ZnO, in general, the residual  $n$ -type conductivity of nominally undoped material in combination with the quasistatic nature of the application and the removal of stress combine to short out any macroscopic piezoelectric effects.<sup>40</sup> In support of this, we note that in the case of electronic transitions such as free and bound excitons in ZnO, reflectance spectra in the literature show no evidence of electric field induced nonlinear shifts, broadening or quenching under [0001] stress even up to stresses of the order of 0.4 GPa (see, e.g., Ref. 19). The expected piezoelectrically induced field in ZnO at such stresses will be  $>1000 \text{ kV/cm}$  based on a simple calculation using well established parameters for ZnO [piezoelectric coefficient,  $d_{33} = 12.4 \times 10^{-12} \text{ C/N}$  (Ref. 41)]. The exciton ionization field in ZnO is  $\sim 300 \text{ kV/cm}$  (Ref. 42) and a highly nonlinear energy shift is expected at such high fields in addition to a significant degree of exciton broadening and quenching.<sup>43</sup> The absence of such effects supports the view that macroscopic piezoelectric effects are quenched in most ZnO crystals (unless deliberately compensated). In other wurtzite materials or highly compensated ZnO samples,<sup>40</sup> the effect of piezoelectrically induced fields on defect energy levels may have to be accounted for in addition to the effects of stress detailed in Sec. III.

There are two further aspects relevant to uniaxial stress studies of defects which remain to be discussed, namely, polarized intensity information for transitions between levels and the effects of stress-induced interactions between different energy levels of the defect.

In most cases experimental measurements involve the study of transitions between energy levels, e.g., between electronic/vibronic energy levels in photoluminescence or

absorption studies. The relative intensities and polarized intensities of the stress-split components of such transitions are also determined by symmetry considerations, and this information is often used in uniaxial stress studies on defects in cubic lattices to supplement the splitting pattern information in order to identify the details of the transition, e.g., the electric dipole direction.<sup>44</sup> Although polarized intensity information is used to supplement the splitting pattern information for defects in cubic crystals for stresses along high symmetry directions, the situation is considerably more complicated in the case of wurtzite crystals. Firstly, wurtzite crystals are uniaxial even in the absence of applied stress and become biaxial for applied stress along any direction other than the  $z$  axis. This means that the (polarized) intensities will vary depending on the viewing direction and there is no unique (polarized) intensity pattern for any stress direction. This situation is similar to that encountered for stresses parallel to  $\langle 110 \rangle$  in the cubic lattice.<sup>26</sup> Additionally, while the viewing direction in most experiments is normal to the stress direction, there is a remaining degree of freedom associated with rotation of the viewing direction about the uniaxial stress direction and no natural choices suggest themselves for the case of stress along an arbitrary direction. The tabulation of all results for all possible transitions and viewing directions, based solely on symmetry considerations, is extremely complex and will not be attempted in this work. This task is in any case generally more suited to a case by case analysis because (a) the results will be dependent on the specific experimental geometry and (b) the details of the dipole orientation at a defect are strongly influenced by the microscopic defect geometry, while symmetry considerations provide only broad constraints. An example which illustrates the latter point is the two transitions at the  $V_{Zn}-H_2$  monoclinic defect [ $3312.2$  and  $3349.6$   $cm^{-1}$  (Ref. 10)] considered in Secs. IV C and IV D above. In both cases, the detailed analysis shown in Refs. 10 and 45 indicates that the dipole is directed along one of the  $V_{Zn}-H-O$  bond directions in the defect (one parallel to the wurtzite  $c$  axis and the other close to perpendicular to the  $c$  axis, both in the  $X-Z$  plane), while the relevant symmetry considerations indicate only that the  $X$  and  $Z$  components of the dipole are nonzero and the  $Y$  component vanishes, and give no further information on the relative magnitudes of the two nonzero components.<sup>10,36,45</sup>

A general analysis of the polarized intensities of the stress-split components is provided by Kaplyanskii for anisotropic (lower symmetry) defects in cubic crystals<sup>26</sup> where one of the principal axes of the uniaxially stressed crystal must be parallel to the stress direction in the cases considered due to symmetry considerations. However, this approach is, in general, not appropriate for wurtzite crystals subjected to uniaxial stress along an arbitrary direction because there is no symmetry requirement for the alignment of the principal axes of the biaxial crystal with the applied stress direction.

We also note in passing that a number of practical effects also tend to reduce the effectiveness of measurements of polarized intensities, particularly for emission spectroscopies. These effects include multiple depolarizing internal reflec-

tions for emission spectroscopies [particularly important for high refractive index materials with large critical angles for total internal reflection such as ZnO and GaN (Ref. 46)] and the rather large collection solid angles generally used in techniques such as photoluminescence, which tend to average over a range of viewing directions and hence over a range of (polarized) intensities.

Finally, the splitting patterns we have calculated have assumed the absence of interactions with higher-lying excited states, and thus the shifts and splittings are linear with applied stress. Clearly, for large applied stresses, some interaction is to be expected with other energy levels of the defect and the splitting patterns may become nonlinear and possibly show anticrossing behavior.<sup>47</sup> However, in the regime of low to intermediate stresses, the splitting patterns derived in Sec. III will describe the behavior of the defect with reasonable accuracy, and the number of stress-split components and the relationship between the measured shift rates should enable an accurate determination of the defect symmetry (particularly if information is available for uniaxial stress along more than one direction or along a low symmetry direction).

The results in Sec. III above therefore enable a determination of the defect symmetry even if interactions are present and (polarized) intensity information is not considered. This basic defect symmetry information may then be used as a first approximation from which a more detailed model may be generated, knowing the viewing direction and the behavior at high levels of uniaxial stress. Refinement of the more detailed model will enable the nature of the transition (e.g., electric dipole direction) and the nature of the interacting excited states to be ascertained.

## VI. CONCLUSIONS

We have given a general analysis, by the application of group-theoretical considerations, of the splitting patterns of all types of energy levels for all symmetry classes of point defects in wurtzite crystals under uniaxial stresses applied along arbitrary crystal directions. We have compared the results of our analyses with data from the literature and have shown that good agreement is found in all the cases considered.

We believe that the analyses given in this paper will be useful in the determination of the symmetry of point defects in wurtzite lattices generally and will provide information which may be used as a reliable starting point for more detailed models incorporating information on transition intensities and stress-induced interaction between levels. Determination of defect symmetries will also enable easy comparison with theoretical, *ab initio*, studies of proposed defect structures.

## ACKNOWLEDGMENTS

We acknowledge financial support from Science Foundation Ireland (Grants No. 02/IN1/I95 and No. 06/RFP/PHY052) and the Irish Higher Education Authority under the NDP.

\*Author to whom correspondence should be addressed; enda.mcglynn@dcu.ie

- <sup>1</sup>D. C. Look, *Mater. Sci. Eng., B* **80**, 383 (2001).
- <sup>2</sup>D. P. Norton, Y. W. Heo, M. P. Ivill, K. Ip, S. J. Pearton, M. F. Chisholm, and T. Steiner, *Mater. Today* **7**, 34 (2004).
- <sup>3</sup>J. W. Orton and C. T. Foxon, *Rep. Prog. Phys.* **61**, 1 (1998).
- <sup>4</sup>X. Q. Wang and A. Yoshikawa, *Prog. Cryst. Growth Charact. Mater.* **48-49**, 42 (2004).
- <sup>5</sup>D. C. Look, D. C. Reynolds, Z.-Q. Fang, J. W. Hemsky, J. R. Sizelove, and R. L. Jones, *Mater. Sci. Eng., B* **66**, 30 (1999).
- <sup>6</sup>D. C. Look, C. Coskun, B. Claffin, and G. C. Farlow, *Physica B* **340-342**, 32 (2003).
- <sup>7</sup>S. Nakamura, S. J. Pearton, and G. Fasol, *The Blue Laser Diode: The Complete Story* (Springer-Verlag, Berlin, 2000).
- <sup>8</sup>S. J. Jokela and M. D. McCluskey, *Phys. Rev. B* **72**, 113201 (2005).
- <sup>9</sup>E. V. Lavrov and J. Weber, *Phys. Status Solidi B* **243**, 2657 (2006).
- <sup>10</sup>E. V. Lavrov and J. Weber, *Phys. Rev. B* **73**, 035208 (2006).
- <sup>11</sup>Y. F. Yan, J. B. Li, S.-H. Wei, and M. M. Al-Jassim, *Phys. Rev. Lett.* **98**, 135506 (2007).
- <sup>12</sup>T. Yamamoto and H. Katayama-Yoshida, *Physica B* **302-303**, 155 (2001).
- <sup>13</sup>S. K. Limpijumngong, S. B. Zhang, S.-H. Wei, and C. H. Park, *Phys. Rev. Lett.* **92**, 155504 (2004).
- <sup>14</sup>Y. Liu, M. Z. Kauser, M. I. Nathan, P. P. Ruden, S. Dogan, H. Morkoç, S. S. Park, and K. Y. Lee, *Appl. Phys. Lett.* **84**, 2112 (2004).
- <sup>15</sup>Y. Liu, M. Z. Kauser, M. I. Nathan, P. P. Ruden, A. M. Dabiran, B. Hertog, and P. P. Chow, *Appl. Phys. Lett.* **81**, 3398 (2002).
- <sup>16</sup>K. S. Wan, A. A. Porporati, G. Feng, H. Yang, and G. Pezzotti, *Appl. Phys. Lett.* **88**, 251910 (2006).
- <sup>17</sup>G. Pezzotti, W. Zhu, A. Leto, A. Matsutani, and A. A. Porporati, *J. Phys. D* **39**, 4975 (2006).
- <sup>18</sup>J. Wrzesinski and D. Fröhlich, *Phys. Rev. B* **56**, 13087 (1997).
- <sup>19</sup>D. W. Langer, R. N. Euwema, K. Era, and T. Koda, *Phys. Rev. B* **2**, 4005 (1970).
- <sup>20</sup>K. Cho, *Phys. Rev. B* **14**, 4463 (1976).
- <sup>21</sup>I. Broser, A. Hoffmann, R. Heitz, and P. Thurian, *J. Lumin.* **48-49**, 693 (1991).
- <sup>22</sup>C. Solbrig, *Z. Phys.* **211**, 429 (1968).
- <sup>23</sup>M. Grynberg, *Phys. Status Solidi* **21**, 255 (1968).
- <sup>24</sup>A. A. Kaplyanskii and A. K. Przhevuskii, *Fiz. Tverd. Tela (Leningrad)* **9**, 257 (1967) [*Sov. Phys. Solid State* **9**, 190 (1967)].
- <sup>25</sup>A. A. Kaplyanskii and A. K. Przhevuskii, *Dokl. Akad. Nauk SSSR* **142**, 313 (1962) [*Sov. Phys. Dokl.* **7**, 37 (1962)].
- <sup>26</sup>A. A. Kaplyanskii, *Opt. Spektrosk.* **16**, 602 (1964) [*Opt. Spectrosc.* **16**, 329 (1964)].
- <sup>27</sup>A. A. Kaplyanskii, *Opt. Spektrosk.* **16**, 1031 (1964) [*Opt. Spectrosc.* **16**, 557 (1964)].
- <sup>28</sup>K. Mohammed, G. Davies, and A. T. Collins, *J. Phys. C* **15**, 2779 (1982).
- <sup>29</sup>K. G. McGuigan, E. McGlynn, F. O' Cairbre, J. Love, and M. O. Henry, *J. Phys.: Condens. Matter* **12**, 7055 (2000).
- <sup>30</sup>R. Sharma, P. M. Pattison, H. Masui, R. M. Farrell, T. J. Baker, B. A. Haskell, F. Wu, S. P. DenBaars, J. S. Speck, and S. Nakamura, *Appl. Phys. Lett.* **87**, 231110 (2005).
- <sup>31</sup>H. L. Zhou, S. J. Chua, H. Pan, Y. W. Zhu, T. Osipowicz, W. Liu, K. Y. Zang, Y. P. Feng, and C. H. Sow, *J. Phys. Chem. C* **111**, 6405 (2007).
- <sup>32</sup>J.-R. Duclère, B. Doggett, M. O. Henry, E. McGlynn, R. T. Rajendra Kumar, J.-P. Mosnier, A. Perrin, and M. Guilloux-Viry, *J. Appl. Phys.* **101**, 013509 (2007).
- <sup>33</sup>B. D. Cullity, *Elements of X-Ray Diffraction* (Addison-Wesley, Reading, MA, 1978).
- <sup>34</sup>R. C. Casella, *Phys. Rev.* **114**, 1514 (1959).
- <sup>35</sup>MATLAB® commercial technical computing language ([www.mathworks.com](http://www.mathworks.com)).
- <sup>36</sup>S. L. Altmann and P. Herzog, *Point-Group Theory Tables* (Oxford University Press, New York, 1994).
- <sup>37</sup>M. Tinkham, *Group Theory and Quantum Mechanics* (McGraw-Hill, New York, 1964).
- <sup>38</sup>A. E. Hughes and W. A. Runciman, *Proc. Phys. Soc. London* **90**, 827 (1967).
- <sup>39</sup>G. Davies and M. H. Nazare, *J. Phys. C* **13**, 4127 (1980).
- <sup>40</sup>A. R. Hutson, *Phys. Rev. Lett.* **4**, 505 (1960).
- <sup>41</sup>D. F. Crisler, J. J. Cupal, and A. R. Moore, *Proc. IEEE* **56**, 225 (1968).
- <sup>42</sup>E. McGlynn, J. Fryar, G. Tobin, C. Roy, M. O. Henry, J.-P. Mosnier, E. de Posada, and J. G. Lunney, *Thin Solid Films* **458**, 330 (2004).
- <sup>43</sup>D. F. Blossey, *Phys. Rev. B* **3**, 1382 (1971).
- <sup>44</sup>L. Jeyanathan, Ph.D. thesis, University of London, 1994.
- <sup>45</sup>E. V. Lavrov, J. Weber, F. Börrnert, Chris G. Van de Walle, and R. Helbig, *Phys. Rev. B* **66**, 165205 (2002).
- <sup>46</sup>O. Madelung, *Semiconductors: Data Handbook* (Springer-Verlag, Berlin, 2003).
- <sup>47</sup>E. McGlynn, M. O. Henry, K. G. McGuigan, and M. C. doCarmo, *Phys. Rev. B* **54**, 14494 (1996).
- <sup>48</sup>CrystalMaker Software, Ltd. (<http://www.crystallmaker.com>).